# Slab-based Faraday isolators and Faraday mirrors for 10-kW average laser power

Efim A. Khazanov

It is shown that the use of slabs instead of rods makes it possible to fabricate Faraday isolators and Faraday mirrors operating at a multikilowatt power. Analytical dependences of thermally induced depolarization in Faraday devices on radiation power and on slab aspect ratio have been obtained.

*OCIS codes:* 140.6810, 230.2240.

## 1. Introduction

The light absorption in Faraday elements generates a temperature distribution that is nonuniform over a transverse cross section. This leads to thermal lensing, nonuniform distribution of the angle of rotation of the polarization plane because of the temperature dependence of the Verdet constant, and linear (eigenpolarizations are linear) birefringence that is due to the photoelastic effect. Aberrations induced by the thermal lens ($dn/dT$ contribution only) do not give rise to polarization distortions and can be effectively compensated with a phase-conjugate mirror[1] or spherical optics.[2–5] The self-induced depolarization of high-power radiation in the magneto-optical rod was first studied in Refs. 6–8, where it was shown that it is the photoelastic effect that makes the greatest contribution to depolarization and that the effect of the temperature dependence of the Verdet constant may be neglected. In Refs. 9 and 10 this theoretical prediction was confirmed experimentally.

In Ref. 8 two novel designs for Faraday isolators were suggested and theoretically investigated for the rod geometry [Figs. 1(b) and 1(c)]. They comprise two Faraday elements, each of them rotating the polarization plane 22.5°, with a reciprocal optical element placed between them. The polarization distortions that a beam experiences while passing the first Faraday element are partially compensated in the second. Further experiments[9,10] confirmed the high efficiency of the novel designs. In Refs. 4 and 11 the influence of laser beam shape and crystal orientation on all three designs of the Faraday isolator was considered. Another method for compensating depolarization in the Faraday isolator was implemented in Ref. 12. It relies on the use of crystalline quartz cut along the optical axis and placed inside a telescope. From Refs. 4 and 8–12 it follows that the most efficient and convenient is a scheme with a reciprocal quartz rotator [Fig. 1(c)]. The first Faraday element and the quartz rotator together rotate the polarization 90° (22.5° + 67.5°). Thus the angle between the polarization incident on the first and the second Faraday elements is exactly 90°, which makes it possible to compensate for polarization distortions.

Unlike isolators, the Faraday mirror does not include any polarizers and is used not for optical isolation but, as a rule, for compensation of birefringence in active elements of high-power laser systems [Fig. 1(d)]. After reflection from the Faraday mirror and a repeated pass through a active element, the linear polarization is restored. Such a method for compensating for the birefringence in active elements was first suggested in Ref. 13 and since then has been effectively used in laser amplifiers,[1,14] oscillators,[2,3,15] regenerative amplifiers,[15] and optical fibers.[16] It is clear that if the Faraday mirror itself inserts polarization distortions (depolarization), then the compensation for birefringence in the active element will be incomplete.

Despite the great similarity between the Faraday mirror and the Faraday isolator, there are two primary differences between them that make it ineffective to use the novel isolator designs [Figs. 1(b) and 1(c)] for the mirror. First, the isolation is governed only by the depolarization in the second pass through

E. A. Khazanov (khazanov@appl.sci-nnov.ru) is with the Institute of Applied Physics, 46 Uljanov Street, Nizhny Novgorod 603950, Russia.

Received 20 June 2003; revised manuscript received 8 December 2003; accepted 19 December 2003.

0003-6935/04/091907-07$15.00/0

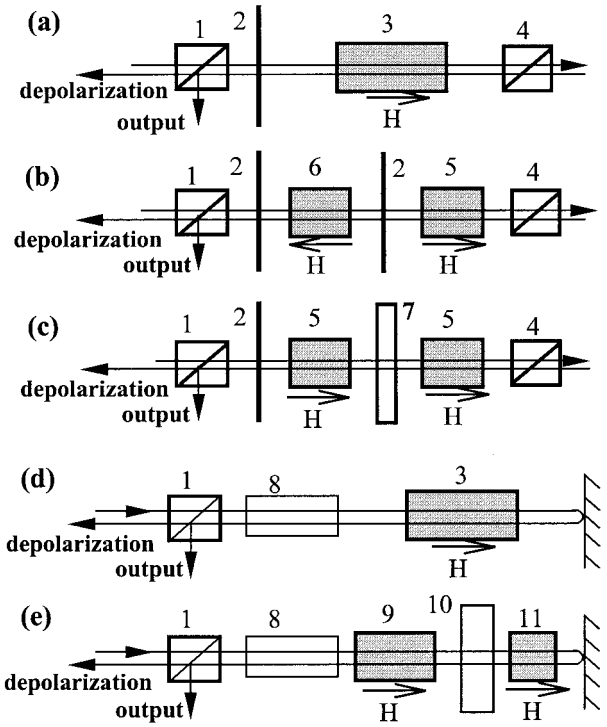


Fig. 1. (a), (d), Traditional and (b), (c), (e) novel designs of (a), (b), (c) Faraday isolator and (d), (e) Faraday mirror. 1, 4, polarizers; 2, $\lambda/2$ plates; 3, 45° Faraday rotator; 5, 22.5° clockwise Faraday rotator; 6, 22.5° counterclockwise Faraday rotator; 7, 67.5° reciprocal polarization rotator; 8, laser active element; 9, 30° Faraday rotator; 10, 90° reciprocal polarization rotator; 11, 15° Faraday rotator.

the isolator, whereas with the mirror the polarization distortions are accumulated during both passes. Second, the radiation that is incident on the isolator is always linearly polarized (we assume ideal polarizers) and also in a certain direction. Therefore for good isolation it is enough that only this linear polarization be a little distorted during the return pass. In contrast, the radiation that is incident on the Faraday mirror has already been depolarized in the active element. A detailed calculation[17] shows that use of the isolator designs presented in Figs. 1(b) and 1(c) for the Faraday mirror can only insignificantly improve its parameters in comparison with the traditional design.

In Ref. 17 a novel design for the Faraday mirror [Fig. 1(e)] was suggested; this design can partially compensate for the depolarization in magneto-optic elements. It was shown that the design in Fig. 1(e) is efficient in compensating for the birefringence in the active element even with a considerable heat release in the magneto-optic elements. Further experiments[18] confirmed the efficiency of this technique.

All the above theoretical and experimental results have been obtained for the rod geometry of the magneto-optical elements and for Gaussian (or super-Gaussian) beams. Summarizing these results, one can conclude that it is quite possible to

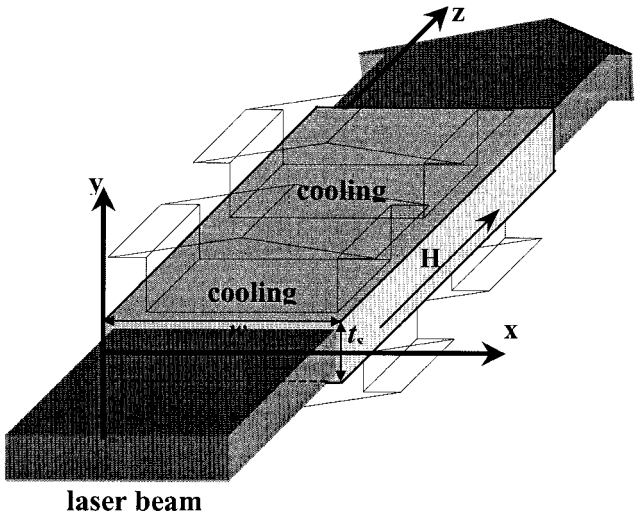


Fig. 2. Use of slabs in Faraday devices.

construct reliable Faraday devices for radiation with average power up to 1 kW. Advancing further to the multikilowatt range requires new approaches related to the use of either several thin discs cooled through an optical surface or slabs and rectangular (elliptical) beams. It is evident that the depolarization in the new designs [Figs. 1(b), 1(c), and 1(e)] will be significantly lower than in the traditional ones [Figs. 1(a) and 1(d)] in any geometry. In this paper the aim is to determine the maximum power that the Faraday devices (both novel and traditional) can withstand when slabs are used. I focus on two main issues: how the depolarization depends on the geometry of slab, and what maximum power the novel designs provide in comparison with the traditional devices.

## 2. Depolarization Ratio of Faraday Devices Based on Slabs

In this section I derive expressions for the depolarization ratio for the rectangular geometry of magneto-optic elements (Fig. 2). The depolarization ratio $\gamma_{\text{slab}}$ for all designs in Fig. 1 was determined as a ratio of radiation power transmitted (from right to left) through polarizer 1 to the radiation power incident upon the polarizer:

$$\gamma_{\text{slab}} = \frac{\int_{-0.5t_s}^{0.5t_s}\int_{0}^{w_s} |\mathbf{E}_1 \cdot \mathbf{x}_0|^2 \mathrm{d}x\mathrm{d}y}{\int_{-0.5t_s}^{0.5t_s}\int_{0}^{w_s} |\mathbf{E}_1|^2 \mathrm{d}x\mathrm{d}y}. \quad (1)$$

Here $\mathbf{E}_1$ is the field incident on polarizer 1. The isolation ratio is the inverse of the depolarization ratio.

The analytical calculation of the temperature distributions and stress tensor in the slab was made under the following assumptions. The input laser

beam has a uniform intensity distribution and linear polarization along the $x$ axis, and the beam size strictly coincides with the size of the slab. Radiation power absorbed over the entire length of the slab is much less than the incident power. Heat was removed only through horizontal surfaces (see Fig. 2). The thickness $t_s$ of the slab is much less than its width $w_s$. Under these conditions eigenpolarizations of the birefringence induced by the photoelastic effect are oriented along the $x$ and $y$ axes for both [001] and [111] orientations. The phase difference between them, $\delta_1 \equiv \delta_x - \delta_y$, is given by the expressions[19]

$$\delta_l = \pi \frac{p}{R_s}\left(\frac{1}{6} - \frac{2y^2}{t_s^{\,2}}\right) \qquad \text{for [001]}, \quad (2)$$

$$\delta_l = \pi \frac{p}{R_s}\left(\frac{1+2\xi}{3}\right)\left(\frac{1}{6} - \frac{2y^2}{t_s^{\,2}}\right) \qquad \text{for [111]}, \quad (3)$$

where

$$R_s = w_s/t_s \quad (4)$$

is the aspect ratio of the slab and

$$p = \frac{L}{\lambda}\frac{Q\alpha P_0}{\kappa}, \quad (5)$$

$$Q = \left(\frac{1}{L}\frac{dL}{dT}\right)\frac{n_0^{\,3}}{4}\frac{1+\nu}{1-\nu}(p_{11}-p_{12}), \quad (6)$$

$$\xi = \frac{2p_{44}}{p_{11}-p_{12}},$$

and $\nu$, $\kappa$, $\alpha$, $(1/L)(dL/dt)$, $n_0$, $p_{i,j}$, and $L$ are the Poison's ratio, thermal conductivity, absorption coefficient, thermal expansion coefficient, refraction index, photoelastic coefficients, and the length of the magneto-optical medium, respectively; $P_0$ and $\lambda$ are the power and the wavelength of the laser radiation heating the slab. Parameter $p$ has the sense of laser power normalized to constants of the magneto-optical medium. The laser power $P_0 = 1$ kW corresponds to parameter $|p| = 1$ for the best terbium gallium garnet (TGG) sample ($\alpha Q = -3.2 \times 10^{-7}$ K$^{-1}$ m$^{-1}$) studied in Ref. 11 and $|p| = 2$ for the average TGG sample from Ref. 11 (we took into account $\kappa = 7.4$ W/Km, $L/\lambda = 24{,}000$). Parameter $\alpha Q$ for TGG crystal from different sources may be found in Ref. 11.

It is obvious from Eqs. (2) and (3) that the [001] orientation is better than [111] because induced birefringence for the [001] is smaller (for a TGG crystal, a magneto-optic crystal most widely used in the wavelength range of 1 $\mu$m, parameters $\xi = 2.25 \pm 0.2$). Further, it is assumed that the crystal has a [001] orientation, but all results for a [111] orientation may be obtained by replacing parameter $p$ with $p(1 + 2\xi)/3$.

The output radiation in all designs shown in Fig. 1 was calculated by the Jones matrix technique. Taking into account the induced thermal birefringence with eigenpolarizations along $x$ and $y$ axes, the matrix of the Faraday element has the form[20,21]

$$F(\delta_c, \delta_l) = \sin\frac{\delta}{2}\begin{bmatrix} \cot\left(\frac{\delta}{2}\right) - i\frac{\delta_l}{\delta} & -\frac{\delta_c}{\delta} \\ \frac{\delta_c}{\delta} & \cot\left(\frac{\delta}{2}\right) + i\frac{\delta_l}{\delta} \end{bmatrix}, \quad (7)$$

where

$$\delta^2 = \delta_1^{\,2} + \delta_c^{\,2};$$

$\delta_c$ is the phase difference for purely circular (in the absence of linear) birefringence. Note that the rotation angle of polarization plane is $\delta_c/2$. The direction of the rotation is determined by the sign of $\delta_c$. When $\delta_c$ is positive, the rotation is anticlockwise. As in Ref. 7, I calculated the influence of the temperature dependence of the Verdet constant. The analysis shows that this effect is negligibly small in comparison with the photoelastic effect discussed here (as in the rod geometry[7]). Thus, let us further assume that $\delta_c$ does not depend on temperature.

The matrices for a half-wave plate with axis angle $\beta_L$ and a reciprocal rotator on angle $\beta_R$ are well known:

$$\mathbf{L}_2(\beta_L) = \begin{bmatrix} \cos 2\beta_L & \sin 2\beta_L \\ \sin 2\beta_L & -\cos 2\beta_L \end{bmatrix},$$

$$\mathbf{R}(\beta_R) = \begin{bmatrix} \cos\beta_R & \sin\beta_R \\ -\sin\beta_R & \cos\beta_R \end{bmatrix}. \quad (8)$$

Knowing the matrices (7), (8) and input field $\mathbf{E}_{in} = E_0\mathbf{x}_0$, one can easily find the field incident on polarizer 1, $\mathbf{E}_1$, for all five design in Figs. 1(a)–1(e):

$$\mathbf{E}_1 = \mathbf{F}(\delta_c = \pi/2, \delta_1)\mathbf{L}_2(3\pi/8)\mathbf{E}_{in}, \quad (9a)$$

$$\mathbf{E}_1 = \mathbf{L}_2(\pi/4)\mathbf{F}(\delta_c = -\pi/4, \delta_1/2) \times \mathbf{L}_2(\pi/8)\mathbf{F}(\delta_c = \pi/4, \delta_1/2)\mathbf{E}_{in}, \quad (9b)$$

$$\mathbf{E}_1 = \mathbf{L}_2(\pi/16)\mathbf{F}(\delta_c = \pi/4, \delta_1/2) \times \mathbf{R}(3\pi/8)\mathbf{F}(\delta_c = \pi/4, \delta_1/2)\mathbf{E}_{in}, \quad (9c)$$

$$\mathbf{E}_1 = \mathbf{F}(\delta_c = \pi/2, \delta_1)\mathbf{F}(\delta_c = \pi/2, \delta_1)\mathbf{E}_{in}, \quad (9d)$$

$$\mathbf{E}_1 = \mathbf{F}(\delta_c = 2\pi/3, 2\delta_1/3)\mathbf{R}(-\pi/2) \times \mathbf{F}(\delta_c = \pi/6, \delta_1/3)\mathbf{F}(\delta_c = \pi/6, \delta_1/3) \times \mathbf{R}(\pi/2)\mathbf{F}(\delta_c = \pi/3, 2\delta_1/3)\mathbf{E}_{in}. \quad (9e)$$

Substituting Eqs. (9) into Eq. (1), one can find the depolarization ratio $\gamma_{\text{slab}}$:

$$\gamma_{\text{slab}} = \frac{1}{45} R_s^{-2} p^2 \cong 2.22 \times 10^{-3} \left(\frac{p}{R_s}\right)^2 \quad \text{for Fig. 1(a),} \quad (10a)$$

$$\gamma_{\text{slab}} = \frac{(\pi - 4\sqrt{2} + 2)^2}{3780} R_s^{-4} p^4 \cong 7.02 \times 10^{-5} \left(\frac{p}{R_s}\right)^4 \quad \text{for Fig. 1(b),} \quad (10b)$$

$$\gamma_{\text{slab}} = \frac{(\pi - 2\sqrt{2})^2}{3780} R_s^{-4} p^4 \cong 2.60 \times 10^{-5} \left(\frac{p}{R_s}\right)^4 \quad \text{for Fig. 1(c),} \quad (10c)$$

$$\gamma_{\text{slab}} = \frac{4}{45} R_s^{-2} p^2 \cong 8.89 \times 10^{-2} \left(\frac{p}{R_s}\right)^2 \quad \text{for Fig. 1(d),} \quad (10d)$$

$$\gamma_{\text{slab}} = \frac{(\pi - 2\sqrt{3})^2}{945} R_s^{-4} p^4 \cong 1.10 \times 10^{-4} \left(\frac{p}{R_s}\right)^4 \quad \text{for Fig. 1(e).} \quad (10e)$$

Here it is assumed that $\delta_1 \ll 1$ and active elements in Figs. 1(d) and 1(e) do not introduce any depolarization; i.e., the values of $\gamma$ given characterize depolarization introduced by the Faraday mirror itself. For comparison I include here formulas obtained in Refs. 4, 8, 17, and 22 for the rod geometry for a crystal with the [001] orientation:

$$\gamma_{\text{rod}} = \frac{A_1}{\pi^2} p^2 \cong 0.0139 p^2 \quad \text{for Fig. 1(a),} \quad (11a)$$

$$\gamma_{\text{rod}} = p^4 \frac{8A_2}{\pi^4} \xi^2 (b^2 - a^2) \cong 6.89 \times 10^{-5} \xi^2 p^4 \quad \text{if } \xi > 1.315 \quad \text{for Fig. 1(b),} \quad (11b)$$

$$\gamma_{\text{rod}} = p^4 \frac{8A_2}{\pi^4} (b^2 + 2a^2) \cong 8.48 \times 10^{-5} p^4 \quad \text{if } \xi = 1 \quad \text{for Fig. 1(b),} \quad (11c)$$

$$\gamma_{\text{rod}} = p^4 \frac{2a^2 A_2}{\pi^4} (3\xi^4 + 2\xi^2 + 3) \cong 1.32 \times 10^{-6} (3\xi^4 + 2\xi^2 + 3) p^4 \quad \text{for Fig. 1(c),} \quad (11d)$$

$$\gamma_{\text{rod}} = \frac{2A_1}{\pi^2} p^2 \cong 0.0278 p^2 \quad \text{for Fig. 1(d),} \quad (11e)$$

$$\gamma_{\text{rod}} = \frac{(2\sqrt{3} - \pi)^2 p^4}{2\pi^4} (3\xi^4 + 2\xi^2 + 3) A_2 \cong 2.24 \times 10^{-5} (3\xi^4 + 2\xi^2 + 3) p^4 \quad \text{for Fig. 1(e),} \quad (11f)$$

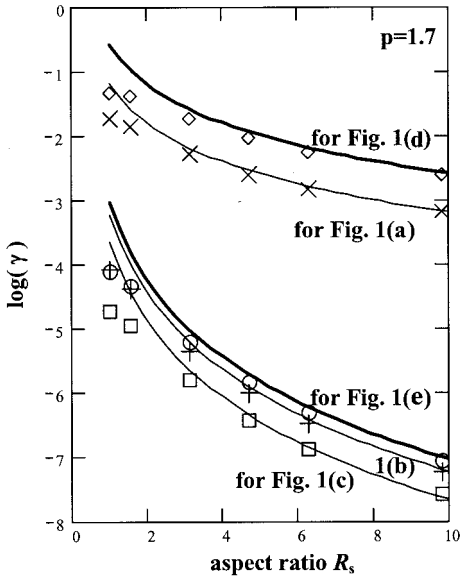


Fig. 3. Analytical (curves) and numerical (points) dependences of depolarization ratio on aspect ratio. For Faraday isolator (thin curves) designs: for Fig. 1(a), crosses; Fig. 1(b), pluses; Fig. 1(c), squares for Faraday mirror (thick lines): Fig. 1(d), diamonds; Fig. 1(e), circles.

where

$$a = \frac{\pi - 2\sqrt{2}}{8}, \qquad b = \frac{2 - \sqrt{2}}{4},$$

$$A_1 = \int_0^\infty \left(\frac{1}{y} - \frac{\exp(-y)}{y} - 1\right)^2 \frac{dy}{\exp(y)} \cong 0.137,$$

$$A_2 = \int_0^\infty \left(\frac{1}{y} - \frac{\exp(-y)}{y} - 1\right)^4 \frac{dy}{\exp(y)} \cong 0.0421.$$

Formulas (10) were derived under two important assumptions: $R_s \gg 1$ and $\delta_1 \ll 1$. Let us consider what happens if these assumptions are violated. First, the numerical calculations made for an arbitrary aspect ratio $R_s$ show that formulas (10) are in a good agreement with numerical results at $R_s > 3$ (see Fig. 3). A typical beam in slab-based lasers has an aspect ration greater than 3, so formulas (10) are useful in most cases even though they were derived with the assumption $R_s \gg 1$.

Second, Fig. 4 presents dependences expressed by Eqs. (10) and (11) (dashed lines) and the results of numerical integration of Eq. (1) for arbitrary $\delta_1$ (solid curves) for all five designs shown in Fig. 1, for both rods and slabs. The dependences are plotted for a TGG crystal with [001] orientation. As is seen from Fig. 4, at low laser power formulas (10) and (11) give good accuracy. Faraday isolators and Faraday mirrors are usually expected to provide a depolarization ratio of $\gamma = 10^{-4} \ldots 10^{-2}$, so formulas (10) and (11) are useful in practice (see Fig. 4). If the accuracy of Eqs. (10) and (11) is not high enough, the exact value

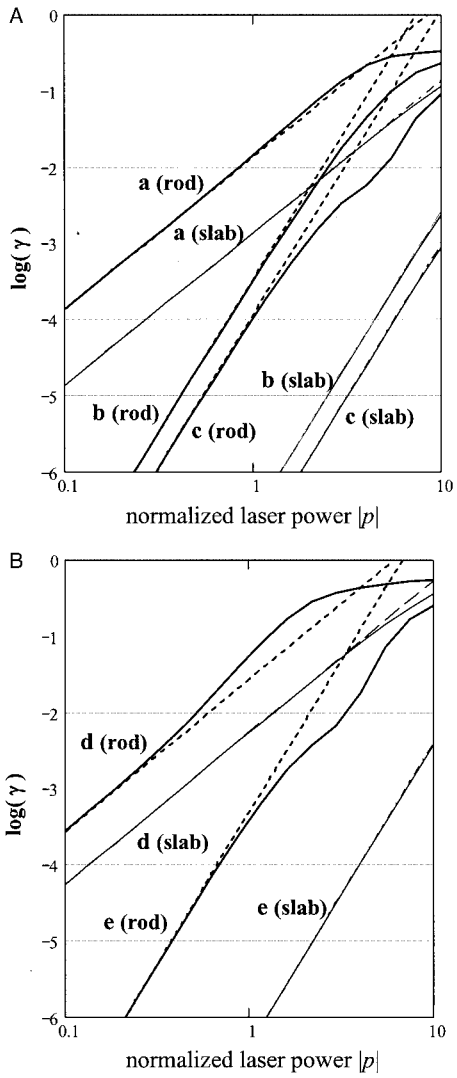


Fig. 4. Analytical (dashed curves) and numerical (solid lines) dependences of depolarization ratio on normalized power $p$ for Faraday isolator designs presented in Figs. 1(a)–1(c) (A) and for Faraday mirror designs presented in Fig. 1(d)–1(e) (B): rod geometry (thick lines) and slab geometry with aspect ratio $R_s = 4$ (thin lines). We assume TGG crystal with the [001] orientation. The laser power $P_0 = 1$ kW corresponds to parameter $|p| = 1$ for the best TGG sample studied in Ref. 11 and $|p| = 2$ for an average TGG sample from Ref. 11.

of the depolarization ratio may be found from Figs. 3 and 4 at any $R_s$ and $\delta_1$.

Figure 4 clearly shows the great advantage of slabs over rods for any optical design as well as the great advantage of new designs [Figs. 1(b), 1(c), and 1(e)] over the traditional ones [Figs. 1(a) and 1(d)] for both geometries.

To conclude this section it would be reasonable to make some comments on thermal-lens and thermal-stress-induced fracture. For uniform heat release and one-dimensional heat conduction (Fig. 2) the slab is a cylindrical lens, which focuses radiation into a line parallel to the long side of the slab. Since the temperature distribution in this geometry is parabolic, the thermal lens is almost nonaberrated (I neglect a small near-edge area here). For estimation of the thermal-lens focus it is quite possible to use a value averaged over two polarizations for a crystal with the [001] orientation without a magnetic field[23]:

$$F = \frac{t_s w_s \kappa}{P_0 L}\left[\frac{\alpha_0}{\frac{dn}{dT} - \left(\frac{1}{L}\frac{dL}{dT}\right)\alpha_T \frac{n_0^3}{4}\frac{1+\nu}{1-\nu}(p_{11}+p_{12})}\right]. \tag{12}$$

Let us estimate the focal length of the thermal lens in the a made of the best TGG sample studied in Ref. 11 [the value in the off shoot of Eq. (12) is $3.2 \times 10^{-6}\ \mathrm{K^{-1}}$ $\mathrm{m^{-1}}$]. For $t_s = 4$ mm, $w_s = 18$ mm, $L/\lambda = 24000$ mm, and laser power $P_0 = 10$ kW, the thermal lens will have a focus of 70 cm. It is important to note that at such short focal lengths it is necessary not only to compensate for the thermal lens by using a cylindrical lens or telescope but also to ensure the same beam size in two slabs and two passes for the designs in Figs. 1(b), 1(c), and 1(e). Otherwise compensation of the depolarization will be incomplete, and expressions (10) will become invalid.

To estimate the fracture limit, let us use the equation for maximum heat power $P_{\max}$ in the slab,[24]

$$P_{\max} = 12 R_T R_s L,$$

where $R_T$ is a thermal-shock parameter. We do not know the value $R_T$ for TGG, but for estimation let us use $R_T = 7$ W/cm (average between $R_T$ for gadolinium scandium aluminum garnet and YAG[24]). Maximum laser power $P_{0\max} = P_{\max}/(\alpha_0 L)$. Assuming $\alpha_0 = 3 \times 10^{-3}$ $\mathrm{cm^{-1}}$ and $R_s = 4$, one can obtain $P_{0\max} = 100$ kW. So the depolarization is the main limit for high-power applications of Faraday isolators and mirrors.

### 3. TGG Ceramics—New Magneto-Optic Material

We predict that the use of Faraday isolators and Faraday mirrors in lasers with high average power will expand considerably over the coming years because of the emergence of polycrystalline ceramics made from TGG. Currently polycrystalline ceramics are used as active elements made of Nd:YAG[25,26] and other cubic crystals,[27] as well as $Q$-switchers.[28] The interest in ceramics is caused by its advantages over single crystals and glass. Specifically, ceramic elements can have apertures of 10 cm and larger, and their thermal conductivity is close to that of a single crystal. This advantage may be particularly important for slab-based Faraday devices and for disc-based[29] ones as well.

Modern technology makes it possible to create ceramic active elements with good optical quality and large apertures. The first samples of TGG ceramics have already been fabricated.[30] Although their optical quality was not high enough, there is no difficulty in principle in fabricating TGG ceramics with high optical quality.[30]

Many properties of ceramics are close to those of

single crystals; however, thermally induced depolarization is somewhat different. The model of depolarization in ceramic active elements with no magnetic field was discussed in Refs. 31 and 32. This model can be generalized for the Faraday isolator and Faraday mirrors, considering the specific features imposed by a magnetic field. The details of this generalization are the subject of ongoing work. In short, we may conclude that if $\delta_1 \ll 1$, all the results obtained for a TGG single crystal with the [111] orientation (the influence of orientation of magneto-optic crystal was studied in detail in Ref. 11) are valid for TGG ceramics as well.

## 4. Conclusion

Based on the analysis of formulas (10) and comparison with formulas (11) (see also Figs. 3 and 4), the following results can be formulated.

1. For the slab geometry (as well as for the rod) the influence of the temperature dependence of the Verdet constant on the depolarization ratio is negligibly small in comparison with the photoelastic effect.
2. In all the schemes shown in Fig. 1 the depolarization ratio is considerably lower when slabs are used in comparison with rods. The depolarization ratio is inversely proportional to the second power of aspect ratio $R_s$ for the traditional designs of the Faraday isolator [Fig. 1(a)] and Faraday mirror [Fig. 1(d)]. The depolarization ratio is inversely proportional to the fourth power of aspect ratio $R_s$ for novel designs of the Faraday isolator (Figs. 1(b) and 1(c)] and the Faraday mirror [Fig. 1(e)].
3. The depolarization ratio in all novel designs is proportional to the fourth power of the laser power and is considerably lower than in traditional designs where the depolarization ratio is proportional to the square of the power.
4. If a [001]-oriented slab with aspect ratio $R_s = 4$ is made of the best TGG crystal studied in Ref. 11, the Faraday isolator presented in Fig. 1(c) provides an isolation ratio of 30 dB at laser a power of 10 kW, whereas the Faraday mirror in Fig. 1(e) yields 24 dB at the same laser power.

In summary, we can conclude that the use of the slab geometry in combination with earlier suggested schemes for depolarization compensation [Figs. 1(b), 1(c), and 1(e)] will make it possible to create Faraday isolators and Faraday mirrors capable of operating at powers up to 10 kW. The emergence of high-quality TGG ceramics will help advance this technology to even higher powers. Slab-based Faraday isolators [designs in Figs. 1(a) and 1(c)] were manufactured at the Institute of Applied Physics. The results of this testing are in preparation for publication.

## References


1. N. Andreev, E. Khazanov, O. Kulagin, B. Movshevich, O. Palashov, G. Pasmanik, V. Rodchenkov, A. Scott, and P. Soan, "A two-channel repetitively pulsed Nd:YAG laser operating at 25 Hz with diffraction-limited beam quality," IEEE J. Quantum Electron. **35,** 110–114 (1999).
2. K. S. Lai, R. Wu, and P. B. Phua, "Multiwatt $KTiOPO_4$ optical parametric oscillators pumped within randomly and linearly polarized Nd:YAG laser cavities," in *Nonlinear Materials, Devices, and Applications*, J. W. Pierce, ed., Proc. SPIE **3928,** 43–51 (2000).
3. M. R. Ostermeyer, G. Klemz, P. Kubina, and R. Menzel, "Quasi-continuous-wave birefringence-compensated single- and double-rod Nd:YAG lasers," Appl. Opt. **41,** 7573–7582 (2002).
4. E. A. Khazanov, "Characteristic features of the operation of different designs of the Faraday isolator for high average laser-radiation power," Quantum Electron. **30,** 147–151 (2000).
5. A. Poteomkin, N. Andreev, E. Khazanov, A. Shaykin, V. Zelenogorsky, and I. Ivanov, "Use of scanning Hartmann sensor for measurement of thermal lensing in TGG crystal," in *Laser Crystals, Glasses, and Nonlinear Materials Growth and Characterization*, Y. Y. Kalisky, ed., Proc. SPIE **4970,** 10–21 (2003).
6. E. A. Khazanov, O. V. Kulagin, S. Yoshida, and D. Reitze, "Investigation of self-induced distortions of laser radiation in lithium niobate and terbium gallium garnet," in *Conference on Lasers and Electro-Optics*, Vol. 6 of 1998 OSA Technical Digest Series (Optical Society of America, Washington, D.C.), pp. 250–251.
7. E. A. Khazanov, O. V. Kulagin, S. Yoshida, D. Tanner, and D. Reitze, "Investigation of self-induced depolarization of laser radiation in terbium gallium garnet," IEEE J. Quantum Electron. **35,** 1116–1122 (1999).
8. E. A. Khazanov, "Compensation of thermally induced polarization distortions in Faraday isolators," Quantum Electron. **29,** 59–64 (1999).
9. E. Khazanov, N. Andreev, A. Babin, A. Kiselev, O. Palashov, and D. Reitze, "Suppression of self-induced depolarization of high-power laser radiation in glass-based Faraday isolators," J. Opt. Soc. Am. B **17,** 99–102 (2000).
10. N. F. Andreev, O. V. Palashov, A. K. Poteomkin, A. M. Sergeev, E. A. Khazanov, and D. H. Reitze, "45 dB Faraday isolator for 100 W average radiation power," Quantum Electron. **30,** 1107–1108 (2000).
11. E. Khazanov, N. Andreev, O. Palashov, A. Poteomkin, A. Sergeev, O. Mehl, and D. Reitze, "Effect of terbium gallium garnet crystal orientation on the isolation ratio of a Faraday isolator at high average power," Appl. Opt. **41,** 483–492 (2002).
12. N. F. Andreev, E. V. Katin, O. V. Palashov, A. K. Potemkin, D. Reitze, A. M. Sergeev, and E. A. Khazanov, "The use of crystalline quartz for compensation for thermally indused depolarization in Faraday isolators," Quantum Electron. **32,** 91–94 (2002).
13. G. Giuliani and P. Ristori, "Polarization flip cavities: a new approach to laser resonators," Opt. Commun. **35,** 109–112 (1980).
14. I. D. Carr and D. C. Hanna, "Performance of a Nd:YAG oscillator/amplifier with phase-conjugation via stimulated Brillouin scattering," Appl. Phys. B **36,** 83–92 (1985).
15. C. A. Denman and S. I. Libby, "Birefringence compensation using a single Nd:YAG rod," in *Advanced Solid State Lasers*, M. M. Fejer, H. Injeyan, and U. Keller, eds., Vol. 26 of OSA Trends in Optics and Photonics Series (Optical Society of America, Washington, D.C., 1999), pp. 608–612.
16. V. M. Gelikonov, D. D. Gusovskii, V. I. Leonov, and M. A. Novikov, "Birefringence compensation in single-mode optical fibers," Sov. Tech. Phys. Lett. **13,** 322–323 (1987).
17. E. A. Khazanov, "A new Faraday rotator for high average power lasers," Quantum Electron. **31,** 351–356 (2001).
18. E. A. Khazanov, A. A. Anastasiyev, N. F. Andreev, A. Voytovich, and O. V. Palashov, "Compensation of birefringence in active elements with a novel Faraday mirror operating at high average power," Appl. Opt. **41,** 2947–2954 (2002).

19. E. M. Dianov, "Thermal distortion of laser cavity in case of rectangular garnet slab," Kratk. Soobsch. Fiz. **8,** 67–75 (1971).
20. M. J. Tabor and F. S. Chen, "Electromagnetic propagation through materials possessing both Faraday rotation and birefringence: experiments with ytterbium orthoferrite," Appl. Phys. **40,** 2760–2765 (1969).
21. A. P. Voytovich and V. N. Severikov, *Lasers with Anisotropic Resonators* (Nauka i Tehnika, Minsk, 1988).
22. E. A. Khazanov, "High-power propagation effects in different designs of a Faraday isolator," in *Optical Pulse and Beam Propagation II*, Y. B. Band, ed., Proc. SPIE **3927,** 359–367 (2000).
23. A. V. Mezenov, L. N. Soms, and A. I. Stepanov, *Thermooptics of Solid-State Lasers* (Mashinostroenie, Leningrad, 1986).
24. W. Koechner, *Solid-State Laser Engineering* (Springer, New York, 1999).
25. I. Shoji, Y. Sato, S. Kurimura, V. Lupei, T. Taira, A. Ikesue, and K. Yoshida, "Thermal-birefringence-induced depolarization in Nd:YAG ceramics," Opt. Lett. **27,** 234–236 (2002).
26. J. Lu, M. Prabhu, J. Song, C. Li, J. Xu, K. Ueda, A. A. Kaminskii, H. Yagi, and T. Yanagitani, "Optical properties and highly efficient laser oscillation of Nd:YAG ceramic," Appl. Phys. B **71,** 469–473 (2000).
27. J. R. Lu, J. H. Lu, T. Murai, K. Takaichi, T. Uematsu, K. Ueda, H. Yagi, T. Yanagitani, and A. A. Kaminskii, "$Nd^{3+}$:$Y_2O_3$ ceramic laser," Jpn. J. Appl. Phys. Part 2 **40,** L1277–L1279 (2001).
28. K. Takaichi, J. R. Lu, T. Murai, T. Uematsu, A. Shirakawa, K. Ueda, H. Yagi, T. Yanagitani, and A. A. Kaminskii, "Chromium doped $Y_3Al_5O_{12}$ ceramics—a novel saturable absorber for passively self-*Q*-switched one-micron solid state lasers," Jpn. J. Appl. Phys. Part 2 **41,** L96–L98 (2002).
29. E. Khazanov, "Investigation of Faraday isolator and Faraday mirror designs for multi-kilowatt power lasers," in *Solid State Lasers XII*, R. Scheps, ed., Proc. SPIE **4968,** 115–126 (2003).
30. A. Ikesue, Japan Fine Ceramics Center, Nagoya, Japan (personal communication, 2002).
31. E. A. Khazanov, "Thermally induced birefringence in Nd:YAG ceramics," Opt. Lett. **27,** 716–718 (2002).
32. M. Kagan and E. Khazanov, "Features of compensation of thermally induced depolarization in polycrystalline Nd:YAG ceramic," Quantum Electron. **33,** 876–882 (2003).